Sustainable, Rapid Repair Utilizing Advanced Cementitious Materials

FINAL REPORT
October 2019

Submitted By:

Ravi Ranade
Assistant Professor

Pinar Okumus
Associate Professor

University at Buffalo
212 Ketter Hall, Buffalo, NY 14260

External Project Managers:

John Picard, PE
Regional Bridge Maintenance Engineer
New York State DOT - Region 5 (Buffalo)

Bijan Khaleghi, PhD, PE
State Bridge Design Engineer
Washington State DOT

In cooperation with

Rutgers, The State University of New Jersey
And
U.S. Department of Transportation
Federal Highway Administration

Disclaimer Statement

The contents of this report reflect the views of the authors, who are responsible for the facts and the accuracy of the information presented herein. This document is disseminated under the sponsorship of the Department of Transportation, University Transportation Centers Program, in the interest of information exchange. The U.S. Government assumes no liability for the contents or use thereof.

The Center for Advanced Infrastructure and Transportation (CAIT) is a Regional UTC Consortium led by Rutgers, The State University. Members of the consortium are Atlantic Cape Community College, Columbia University, Cornell University, New Jersey Institute of Technology, Polytechnic University of Puerto Rico, Princeton University, Rowan University, SUNY - Farmingdale State College, and SUNY - University at Buffalo. The Center is funded by the U.S. Department of

1. Report No.	2. Government Accession No.	3. Recipient's Catalog No.	
CAIT-UTC-REG 2B			
4. Title and Subtitle Sustainable, Rapid Repair Utilizing Advanced Cementitious Materials		5. Report Date Oct 16, 2019 6. Performing Organization Code CAIT/University at Buffalo	
7. Author(s) Ravi Ranade http://orcid.org/0000-0001-6030-8371, Pinar Okumus https://orcid.org/0000-0002-2197-3261, Hanmin Wang https://orcid.org/0000-0001-5834-1930		8. Performing Organization Report No. CAIT-UTC-REG 2B	
9. Performing Organization Name and Address University at Buffalo 212 Ketter Hall, Buffalo, NY 14260		10. Work Unit No. 11. Contract or Grant No. 69A3551847102	
12. Sponsoring Agency Name and Address Center for Advanced Infrastructure and Transportation Rutgers, The State University of New Jersey 100 Brett Road Piscataway, NJ 08854		13. Type of Report and Period Covered Final Report 10/01/2018 – 09/30/2019 14. Sponsoring Agency Code	
15. Supplementary Notes U.S. Department of Transportation/OST-R 1200 New Jersey Avenue, SE Washington, DC 20590-0001			

16. Abstract

Durability and resilience of a structure are typically considered separately, as they address structural performance under different types of loads. A systematic framework for combined durability-resilience assessment of an RC bridge column is presented in this article. Corrosion of steel reinforcement is the main deterioration mechanism considered for durability evaluation, and earthquakes are assumed to be the primary hazard for resilience assessment. An example bridge column with two types of cover materials – conventional concrete and ductile fiber-reinforced concrete – is considered in our study. The ductile fiber-reinforced concrete provides better durability than the conventional concrete, resulting in lower rebar mass loss at a given time. Fick's second law of diffusion is used to model the corrosion initiation phase. A pitting corrosion model, accounting for the effects of cracking on the corrosion rate, is considered for the corrosion propagation phase. Seismic fragility curves are constructed by nonlinear dynamic analysis, incorporating the rebar mass loss, at discrete times during the life span of the bridge. The results indicate that corrosion of reinforcement increases the vulnerability of the bridge column to seismic hazard. Furthermore, better durability provided by the ductile fiber-reinforced concrete cover leads to improved seismic resilience.

17. Key Words	18. Distribution Statement		
Seismic resilience; Deterioration; Corrosion rate; Cracking; Engineered Cementitious Composite (ECC); Fragility; Service life			
19. Security Classification (of this report) Unclassified	20. Security Classification (of this page) Unclassified	21. No. of Pages 31	22. Price

Form DOT F 1700.7 (8-69)

Acknowledgments

This research was financially supported by the Region 2 University Transportation Center, which is funded by the US Department of Transportation and by University at Buffalo (UB), the State University of New York. Financial support was also provided by the Institute of Bridge Engineering at UB. These financial supports are gratefully acknowledged. The opinions, findings and views expressed in this study are the ones of the authors only and do not necessarily reflect the views, policies, standard specifications or regulations of the parties acknowledged above. Funding agencies do not assume any liability for the contents or the use thereof.

Table of Contents

List of Figures

List of Tables

NOMENCLATURE

Due to the large number of variables used in this article, the following nomenclature is used for parameters in this study:

$C_{CI}(x,t)$	Chloride concentration at spatial coordinate x and time t
C_s	Chloride content at the outer surface of concrete
D_{CI}	Effective chloride diffusion coefficient
erf(.)	Error function
$A(t)$	Rebar area at time t
D_0	Original Rebar diameter
$P(t)$	Pit depth
θ_1	Parameter depending on D_0, $P(t)$, and b in pitting corrosion model
θ_2	Parameter depending on D_0, $P(t)$, and b in pitting corrosion model
b	Width of the pit area
A_1	Parameters depending on D_0, $P(t)$, θ_1 and b in pitting corrosion model
A_2	Parameters depending on D_0, $P(t)$, θ_2 and b in pitting corrosion model
R	Pitting factor
$\lambda(t)$	Corrosion rate in mm/year
$\lambda(t)_{bfcrack}$	Corrosion rate before cracking
$\lambda(t)_{afcrack}$	Corrosion rate after cracking
i_{corr}	Current density
$f(t)$	Yield strength of corroded rebar at time t
f_0	Yield strength of non-corroded reinforcement
Q_{corr}	Percent weight loss (or area loss) of rebar
A_0	Original rebar area
P_{corr}	Internal pressure caused by rust expansion
m_{loss}	Percent of rebar mass loss (or area loss per unit length) due to corrosion
ν	Poisson's ratio
E	Elastic modulus
C	Thickness of concrete cover
σ	Circumferential stress
δ_0	Thickness of the porous zone
δ_c	Radial displacement
r_i	Radius of rebar
r_0	Radius of the thick-wall cylinder (concrete cover)
r	Distance from the center of the thick-wall model to the interface between the rust and concrete
$W(t)$	Crack width of concrete cover at time t
$W(t)_{ECC}$	Crack width of ECC cover at time t
$\Delta A(t)$	Cross-sectional area loss of reinforcement at time t
t_{cr}	Crack initiation time
M_r	Mass of rust per unit length of one rebar
M_{loss}	Mass loss of steel per unit length consumed to produce rust
ρ_r	Mass density of rust
ρ_s	Mass density of the original (non-corroded) steel
ε^*	Tensile strain of ECC

$C_{CI}(x,t)$	Chloride concentration at spatial coordinate x and time t
ε	Tensile strain of ECC in percent
T_1	Time when the peak corrosion rate is reached
$\Phi(.)$	Standard normal cumulative distribution function (CDF)
IM_i	Ground motion intensity measure
$\bar{\theta}$	Parameter of standard normal distribution
$\bar{\beta}$	Parameter of standard normal distribution
EDP	Engineering demand parameter
d	Limiting value of EDP used to define a damage level
$\rho(t)$	Volumetric ratio of transverse rebar at time t
$f_t(t)$	Yield strength of transverse rebar at time t
ε_{cu}	The maximum compressive strain in the confined concrete
ε_{su}	Strain in transverse rebar at ultimate strength
$f_{cc}(t)$	Compressive strength of confined concrete at time t
m	Number of ground motion intensity level
z_j	Number of records which reach a particular damage state in the j^{th} IM level
n_j	Total ground motion records run at j^{th} ground motion intensity levels

1. PROBLEM DESCRIPTION

Reinforcement corrosion in highway bridges is one of the most common durability problems across the world. In the United States, the annual direct cost of repair and maintenance of deteriorating bridges due to corrosion is estimated to be $8.3 billion (*1*). This cost is expected to increase in the future as bridges continue to age (*2*). In addition to its impact on the economy and bridge service life, rebar corrosion can also affect the safety of the structure when a repair is overdue due to budget constraints. An extreme event such as an earthquake, a large vehicular impact, or a hurricane can inflict more damage on a corroded bridge as compared to a sound bridge due to reduction of the buffer capacity.

A systematic computational framework to evaluate the influence of durability (or lack thereof) on the resilience of reinforced-concrete bridges is presented in this report. Although there can be several factors affecting the durability of a reinforced-concrete (RC) bridge, corrosion of steel reinforcement is considered as the primary deterioration mechanism in our study. Earthquakes are assumed as the primary hazard for resilience assessment. An RC bridge column with two types of cover materials – conventional concrete and ductile fiber-reinforced concrete – is considered as an example structure for the demonstration of the framework. The ductile fiber-reinforced concrete in our study is called Engineered Cementitious Composite (ECC), which provides better protection from corrosion than the conventional concrete, resulting in lower rebar mass loss at a given time (*3*).

In the past few decades, several studies have investigated the combined effects of corrosion and seismic hazards on RC infrastructure. Choe et al. (*4*) developed analytical fragility curves for a corroded bridge column using probabilistic methods. Akiyama and Frangopol (*5*) considered the airborne chloride in seismic fragility analysis. Ghosh and Padgett (*6*) presented a computational model for an entire bridge, including the corrosion effects on bridge bearings. Alipour et al. (*7*) performed a life-cycle cost analysis of deteriorated bridges. All of these studies assumed uniform corrosion of steel in chloride-rich environments. However, pitting corrosion is the most commonly observed corrosion mechanism in real RC bridges and its effects on the seismic response of bridges must be incorporated (*8-13*). As the structural capacity changes due to corrosion, the thresholds of engineering demand parameters (e.g., lateral drift) used to define damage states in fragility analysis also change with time, which is captured only by a few researchers (*11, 12, 14*).

Despite the above studies on combined durability-resilience assessment of RC structures, a couple of crucial knowledge gaps still exist. First, the effects of cracks in concrete on the corrosion rate have been considered only by a few researchers (*13*). Corrosion-induced cracks in concrete cover increase the corrosion rate significantly (*15, 16*), and therefore ignoring their effect may cause underestimation of

corrosion effects (*13*). Second, none of the previous studies investigated materials similar to ECC, with superior corrosion resistance compared to the conventional concrete, for the dual purpose of corrosion-mitigation and improving seismic resilience. The framework presented in this report explicitly captures the effects of cracking and incorporates the behavior of ECC into the corrosion model.

ECC is an ultra-ductile concrete with tensile strain capacity of about 300 times that of conventional concrete (*17*). Instead of forming large cracks similar to concrete, it absorbs damage through the formation of micro-cracks of widths (or openings) less than 100 μm even at large imposed deformations well beyond its elastic limit. The compressive strength of ECC is similar to that of a moderate strength concrete (40-50 MPa). Previous researches on the transport properties of ECC suggest that this material, even when strained in tension up to 3%, exhibits water permeability and effective chloride ion diffusivity comparable to uncracked concrete, by the virtue of its intrinsically tight crack width (*18-22*). The difference in performance between ECC and concrete is more significant during the corrosion propagation stage, as ECC can resist the tensile hoop stresses created around the rebars by the expansive corrosion products. Recent research (*22*) has shown the effectiveness of using precast ECC covers for reducing corrosion rates in chloride-rich environments. The ECC properties used in this research are representative of the mix number M45 in Wang and Li (*23*).

The objective of this research is to develop and demonstrate a quantitative tool (a computational framework) to determine the influence of improved structural durability, enabled by the use of an advanced concrete material, on the resilience of RC infrastructure. The computational framework consists of two parts: corrosion model and seismic fragility analysis. In the methodology section of this report, corrosion initiation and propagation models are defined for concrete and ECC, considering crack width effects on corrosion rate. Then, a seismic fragility analysis, incorporating corrosion effects, is introduced. Finally, the computational framework is demonstrated using an example bridge column that uses two alternative cover materials: concrete and ECC.

2. APPROACH

An analytical investigation was used to establish a framework that can combine the effects of deterioration with the effects of seismicity. Behavior of bridge columns under both corrosion and seismic hazards was determined using analytical means based on transport phenomena and structural mechanics, respectively. The framework is applied to an example bridge column to demonstrate its use.

The computational framework presented in this report consists of two separate models– one for corrosion and the other for non-linear dynamic structural analysis of the structural member (a bridge column in this case). In the corrosion model, the time to corrosion initiation is determined using the Fick's second law of diffusion. The time to cracking is determined using the concrete cover's tensile strength. A new crack width-dependent model to determine corrosion rate as a function of time is proposed in this research to enable comparison of concrete with fiber-reinforced cementitious materials that have a better control of crack widths. The output of the corrosion model – the rebar mass loss (for both longitudinal and transverse rebars) as a function of time – is fed into the structural model to update the section properties with time. In the structural model, a set of ground motions is first selected and scaled appropriately. A finite element model (in OpenSEES in this report) of the structural member is used to perform non-linear dynamic structural analysis and determine the engineering damage parameter (EDP) (e.g. drift) as a function of the earthquake intensity [characterized by the peak ground acceleration (PGA)]. A damage measure in terms of the EDP is then used to discretize the damage levels. Finally, the fragility curves (probability of exceeding a certain EDP as a function of earthquake intensity) are constructed at discrete times, which informs the bridge owner about the resilience of a bridge deteriorated by corrosion.

3. METHODOLOGY

3.1 CORROSION MODEL

Chloride-induced corrosion is the major cause of bridge degradation in the US, particularly in the northern states. It happens in two phases: initiation and propagation. In the initiation phase, chloride ions from the outside environment gradually ingress through the concrete cover to steel reinforcement surface. Once the chloride concentration at the reinforcement surface reaches a critical level, active rebar corrosion starts, which marks the beginning of the corrosion propagation phase. The cross-sectional areas of the transverse and longitudinal rebars decrease in the propagation phase due to corrosion. As the rust expands, it generates tensile stress in the surrounding concrete. The concrete cover cracks when the tensile stress reaches the tensile strength of concrete.

3.1.1 Corrosion initiation

The time to corrosion initiation is typically determined using the Fick's second law of diffusion, which is a complex partial differential equation. Time to corrosion initiation can be calculated using Crank's solution (*24*) given in **Equation 1**.

$$C_{CI}(x,t) = C_s\left[1 - \text{erf}\left(\frac{x}{2\sqrt{D_{CI}\,t}}\right)\right] \quad (1)$$

3.1.2 Corrosion propagation

Active corrosion of steel reinforcement happens during the corrosion propagation phase. Corrosion can either occur uniformly throughout a rebar due to the formation of a *corrosion macro-cell* or occur locally due to the formation of a *corrosion micro-cell* or a *pit (25)*. Chloride ion diffusion typically leads to local or pitting corrosion, which is considered in our study. Corrosion products apply radially outward pressure due to their expansive nature, as their volume is about 3-6 times that of the original steel. However, the start of the corrosion propagation phase does not damage the concrete cover right away, as discussed below.

The corrosion propagation phase can be further divided into four stages. In the first stage, the corrosion products fill the porous zone at the rebar-concrete interface without causing any stress in the surrounding concrete. Once the pores are saturated, in the second stage, the corrosion products start to apply outward radial pressure causing tensile hoop stress in the surrounding concrete. This continues until the tensile stress in concrete reaches its tensile strength at which point the cover cracks, marking the end of the second stage. In the third stage, the corrosion rate increases due to increase in the number of cracks as well as increase in the widths (openings) of the existing cracks. In the fourth stage, after reaching a certain crack width, the corrosion rate stabilizes as the built up corrosion products shield the rebar core from extremely rapid corrosion. All the above stages of corrosion are captured in our model.

3.1.2.1 Pitting corrosion

During pitting corrosion, a rebar's cross-sectional area will continuously decrease over time. As discussed above, pitting corrosion is typically observed in real RC structures during the corrosion propagation stage. As name suggests, pitting corrosion creates a pit starting at the surface of the rebar. Unlike uniform corrosion that reduces rebar area throughout the length of the rebar; in pitting corrosion, the rebar mass loss is local as the depth of the pit becomes larger with time. Val and Melchers (*26)* proposed a hemispherical model to simulate pitting corrosion as shown in **Figure 1**.

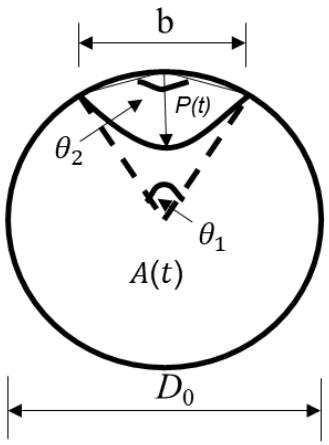

Figure 1 Pitting corrosion (26)

The rebar area, A(t), at time t after corrosion initiation and can be estimated using **Equation 2** (*26*):

$$A(t)_{pitting} = \begin{cases} \frac{\pi {D_0}^2}{4} - A_1 - A_2, & P(t) \le D_0 \frac{\sqrt{2}}{2} \\ A_1 - A_2, & D_0 \frac{\sqrt{2}}{2} < P(t) \le D_0 \\ 0, & P(t) > D_0 \end{cases} \quad (2)$$

The parameters A_1 and A_2 are parameters that can be estimated by the following equations (*26*):

$$A_1 = 0.5\left[\theta_1 \left(\frac{D_0}{2}\right)^2 - b\left|\frac{D_0}{2} - \frac{P(t)^2}{D_0}\right|\right] \quad (3)$$

$$A_2 = 0.5\left[\theta_2 P(t)^2 - b\frac{P(t)^2}{D_0}\right] \quad (4)$$

$$\theta_1 = 2\arcsin(\frac{b}{D_0}), \theta_2 = 2\arcsin(\frac{b}{2P(t)}) \quad (5)$$

$$b = 2P(t)\sqrt{1 - \left(\frac{P(t)}{D_0}\right)^2} \quad (6)$$

The pitting depth, $P(t)$, is be expressed by **Equation 7** (*26*):

$$P(t) = R\int_{t_{corr}}^{t} \lambda(t)dt \quad (7)$$

where, $\lambda(t)$ is the corrosion rate, expressed as:

$$\lambda(t) = 0.0116 \times i_{corr} \quad (8)$$

In addition to the reduction in rebar area, pitting corrosion also causes reduction in yield strength as expressed by Equation (9) (*27*):

$$f(t) = (1.0 - 0.005Q_{corr})f_0 \quad (9)$$

where, Q_{corr} is the percent weight loss (or area loss) of rebar expressed as:

$$Q_{corr} = \frac{A_0 - A(t)}{A_0} * 100 \quad (10)$$

3.1.2.2 Crack initiation time

The buildup of rust causes tensile stress to increase with time in the concrete surrounding the rebar. When this stress reaches the tensile strength of concrete, a crack forms in the concrete cover. Assuming that all the corrosion products remain inside, the rebar mass loss computed below can be converted into internal radial pressure caused by rust expansion using **Equations 11**, **12 and 13** (*28*). In our study, *E* is assumed the same for concrete and ECC (equal to 30 GPa), and C is taken as 60 mm. Concrete around the rebar is modeled as a thick-walled cylinder, in which the circumferential stress can be calculated using **Equation 14**. For simplifying the model, the entire cover is assumed to crack instantaneously when the tensile stress in the circumferential direction at the interface between the rust and concrete reaches the tensile strength of the concrete. As the rebar mass loss (m_{loss}) is a function of time, crack initiation time can be calculated using these equations.

$$m_{loss} = Q_{corr} \times unit\ thickness\ of\ section\ (1\ mm) \quad (11)$$

$$P_{corr} = \frac{m_{loss} E D_0}{90.9(1+\nu+\psi)(D+2\delta_0)} - \frac{2\delta_0 E}{(1+\nu+\psi)(D_0+2\delta_0)} \quad (12)$$

$$\psi = \frac{{D_0}^2}{2C(C+D_0)} \quad (13)$$

$$\sigma = \frac{P_{corr} {r_i}^2}{{r_0}^2 - {r_i}^2}\left[1 + \frac{{r_0}^2}{r^2}\right] \quad (14)$$

3.1.2.3 Time-dependent crack width

After crack initiation, crack width gradually increases with time. Due to different crack control abilities of concrete and ECC, two different time-dependent crack width models are introduced. For concrete, equation (14) (*29*) is used:

$$W(t) = 0.0575\ (\Delta A(t) - \Delta A(t_{cr})) \quad (15)$$

Similar to **Equation 15**, an empirical equation describing the time-dependent crack width of ECC as a function of rebar area (or mass) loss was derived in our study. For this purpose, three relationships were needed: (1) the relation between rebar area loss and outward radial displacement caused by expansive corrosion products, (2) the relation between the outward radial displacement and average hoop strain in the

cover, and (3) the relation between average hoop strain and average crack width of ECC. As mentioned above, unlike concrete, the crack width in ECC is controlled by the bridging fibers. These three relationships are determined as follows.

Considering the densities of original steel and corrosion products and the rebar diameter, a model proposed by Maaddawy and Soudki (*28*) is used to calculate the relationship between outward radial displacement (δ_c) and rebar mass loss, which is given in **Equation 16**. In our study, the ratio of ρ_r to ρ_s is assumed to be 0.5 (*30, 31*) and the ratio between M_{loss} to M_r is assumed to be 0.622 (*28*).

$$\frac{M_r}{\rho_r} - \frac{M_{loss}}{\rho_s} = \pi D_0(\delta_0 + \delta_c) \tag{16}$$

Fakhri (*22)* performed experiments to investigate the relationship between outward radial displacement and average hoop strain of ECC. In these experiments, radial pressure was applied on four hollow ECC cylinders, simulating the effects of rust expansion on the ECC cover. Average strain at the outer surface of ECC cylinders was recorded at three locations. In our study, the relationship between outward radial displacement and average hoop strain is calculated through linear regression on the experimental data reported by Fakhri (*22)* which is given in **Equation 17**:

$$\varepsilon^* = 0.009\delta_c + 3.6 \times 10^{-5} \tag{17}$$

In another experimental study, Ranade et al. (*32*) determined the relationship between the tensile strain and average crack width of ECC. A lognormal probability density function was used to define the observed crack width distribution. In this study, only the mean crack width given in Ranade et al. (*32*) is used for computational efficiency. The relationship between crack width and tensile strain of ECC is given by **Equation 18**. Using **Equations 16**, **17**, and **18** simultaneously, an empirical relation between rebar mass loss due to corrosion and average crack width in ECC was developed.

$$W(t)_{ECC} = 36.1\varepsilon^3 - 101.0\varepsilon^2 + 105.8\varepsilon + 23.8 \tag{18}$$

where, $\varepsilon = \varepsilon^* * 100$

3.1.2.4 Corrosion rate

Previous studies (*15, 16, 21, 22, 33*) have showed that the existence of cracks in both ECC and concrete increases the corrosion rate significantly, depending on the crack width. This is because cracks in the cover provide easier ingress path for water, oxygen, and chloride ions. As explained above, corrosion

propagation can be divided into four stages (*16*). In stages 1 and 2, the corrosion rate is constant prior to crack initiation. In stage 3, after cracking of the concrete cover, corrosion rate increases with increase in number and widths of the cover cracks. Due to lack of experimental data and ease of numerical analysis, the corrosion rate is assumed to increase linearly with time in our study. Other studies (*13*) have also used a similar assumption. In stage 4, corrosion rate reaches a peak value and remains constant thereafter, when the cover crack width reaches a critical value depending on the material.

The time when the critical crack width is reached is iteratively determined using the following steps:

1. Assume the slope ($d\lambda/dt$) of the linear increase in the corrosion rate with time to calculate the time-dependent corrosion rate [$\lambda(t)$] after crack initiation.
2. Calculate the time T_1 when the corrosion rate reaches its peak value for a given material, and determine the corresponding rebar area loss at T_1.
3. Calculate the crack width at T_1 using the relation between rebar mass loss and crack width of the material, as discussed in Section: *Time-dependent crack width.*
4. Check if the crack width reaches the critical crack width for the material at T_1. If yes, the assumed $d\lambda/dt$ and the corresponding time T_1 is correct; else, vary $d\lambda/dt$ and start again from step 1 until this check is satisfied.

3.1.3 Corrosion model properties for the example bridge column

3.1.3.1 Conventional concrete cover

Corrosion initiation phase: In this study, the example bridge is assumed to be a new bridge, and therefore, the initial chloride concentration in the cover concrete is assumed zero. The salt exposure is assumed similar to the urban highway bridges around the authors' university (Western New York). The surface chloride concentration (C_s) based on the database of the Life-365™ (*34)* is taken as 19.8 kg/m^3. The chloride diffusion coefficient (D_{CI}), calculated considering the temperature effects of this area, is 4.50×10^{-12} m^2/s for conventional concrete (*34*). The critical chloride content for corrosion initiation at the rebar-concrete interface is assumed to be 1.2 kg/m^3 (*34*).

Corrosion rate: A *moderate* corrosion rate of 0.0174 mm/year suggested in the literature (*25*) and (*35*) is assumed prior to crack initiation. Due to the lack of peak corrosion rate data in real bridges, the peak corrosion rate after crack initiation is assumed to be 0.0267 mm/year. This value is based on the assumption that longitudinal rebar area would reduce by 20% under moderate corrosion at the end of the service life

(75 years), assuming no repair is performed during the bridge's service life. The critical crack width beyond which the corrosion rate becomes constant is assumed to be 0.2 mm for concrete (*13*).

In our study, it is assumed that when the crack width reaches 1.0 mm, the cover concrete becomes ineffective for carrying seismic loads, and therefore, it is removed from the dynamic structural analysis (*36*).

3.1.3.2 ECC cover

Corrosion initiation phase: The environmental exposure for the ECC cover is the same as that for the conventional concrete cover. Therefore, surface chloride concentration (C_s), temperature variation (that affects D_{Cl}), and initial chloride concentration are same as those for the conventional concrete. The effective chloride diffusion coefficient for the ECC considered in our study is 0.64 times that of conventional concrete (*19*). Although the critical chloride content changes with the type of concrete, its value for ECC is assumed the same as that for concrete due to limited experiment data.

Corrosion rate: Average corrosion rate of the ECC considered in this study is 0.72 times that of conventional concrete based on experimental data (*22*). Thus, the corrosion rates before and after cracking of ECC are taken as 0.0125 mm/year and 0.0192 mm/year in our study, respectively. Average crack widths in ECC are typically limited to 0.1 mm by the fibers. Some experimental data suggests that the corrosion rate in ECC can become constant at crack widths less than 0.1 mm (*22*). However, due to limited experimental data, the corrosion rate is assumed to become constant after the crack width reaches 0.1 mm.

Table 1 summaries all the parameters used in the corrosion model of the example column. All assumed values can be changed in the future based on field data for other columns. The computational framework will remain unchanged regardless of the properties chosen.

Table 1 Parameters considered in the corrosion model of the example bridge column

Parameters	Conventional concrete	ECC	Source
C_s (kg/m^3)	19.8	19.8	(*34*)
D_{CI} (m^2/s)	4.50×10^{-12}	2.86 x 10 $^{-12}$	(*34*)
Critical chloride content at rebar surface (kg/m^3)	1.2	1.2	(*34*)
$\lambda(t)_{bfcrack}$ (mm/year)	0.0174	0.0125	(*25, 35*)
$\lambda(t)_{afcrack}$(mm/year)	0.0267	0.0192	**Explained above**
Critical crack width (mm)	0.2	0.1	(*13*)
ν	0.18	0.18	(*28*)
δ_0 (mm)	20×10^{-3}	20×10^{-3}	(*28*)

3.2 SEISMIC FRAGILITY OF CORRODED BRIDGE COLUMN

3.2.1 Fragility analysis

Seismic fragility curves have found widespread use in probabilistic seismic risk assessment of highway bridges. A fragility curve provides the probability of a structure exceeding a specified level of damage as a function of ground motion intensity measures such as peak ground acceleration (PGA) or spectral acceleration at the geometric mean of the longitudinal and transverse periods. A seismic fragility curve is commonly modeled by a lognormal cumulative distribution function as shown in **Equation 19.** In this equation, $\bar{\theta}$ and $\bar{\beta}$ are estimated from statistical analysis of the damage data. EDP is an engineering demand parameter (e.g. interstory drift, beam plastic rotation, derived damage index, etc.) that is obtained from structural analysis.

$$P(EDP \geq d|IM = IM_i) = \Phi\left[\frac{\ln(IM_i)-\bar{\theta}}{\bar{\beta}}\right] \tag{19}$$

It should be noted that there are multiple methods to create fragility curves and steps may vary between various methods. The following five steps were followed for constructing fragility curves in this report:

1. Select ground motion records for the site of the structure,
2. Develop a structural (finite element) model,
3. Perform incremental dynamic analysis (IDA) for the selected ground motions,
4. Define/select a suitable damage index, and
5. Estimate parameters of fragility curves using statistics.

The details of the steps (1) and (2) are discussed in Section 3.3 as applied to the example bridge column. The details of steps (3) to (5) are given in the following sections.

3.2.2 Incremental dynamic analysis (step 3)

In this paper, IDA proposed by Vamvatsikos and Cornell (*37)* is performed. This involved a large number of nonlinear response history analyses using ground motions that are systematically scaled to increasing earthquake intensities (PGA) until each damage level occurs. IDA yields a distribution of results at varying PGAs that is used to generate a fragility curve. Response history analyses can be performed using any structural analysis software. In this research, the open source structural analysis software is used. Analyses included isolated bridge piers subjected to ground motions.

3.2.3 Time-dependent damage states and damage index (step 4)

The levels of damage are characterized by discrete damage states defined by certain thresholds of a *damage measure*. Although many definitions of damage exist in the literature, in this research, *displacement ductility* is used as the damage measure. Displacement ductility is defined as the ratio of the peak lateral displacement (obtained from the dynamic analysis) to the yield displacement. The yield displacement is defined as the lateral displacement corresponding to the yielding of the outermost longitudinal rebar under tension. Four damage states are defined as follows:

1. Slight Damage: Slight damage is assumed to occur when the peak lateral displacement is equal to the yield displacement. At this level, concrete cover is assumed to have visible cracks under earthquake load near the maximum moment locations.
2. Moderate Damage: Moderate damage is assumed to occur when the maximum compressive strain in the concrete core (confined by steel reinforcement) at column base reaches 0.002 (*11*). At this strain, concrete cover near the bottom of a bridge column is assumed to have minor spalling.
3. Extensive Damage: Extensive damage is defined when the column reaches the displacement ductility that is equal to the geometric mean of the displacement ductility corresponding to the moderate damage state and the collapse state, similar to other studies (*11*).
4. Collapse: Collapse is defined to occur when the maximum compressive strain in the confined concrete reaches ε_{cu} calculated in **Equation 20** (*38*). This value of strain in concrete corresponds to the fracture of the first transverse tie (*11, 12*).

$$\varepsilon_{cu} = 0.004 + \frac{1.4\rho_s f_t(t)\varepsilon_{su}}{f_{cc}(t)} \tag{20}$$

3.2.4 Statistical method to estimate the parameters of fragility curves (step 5)

In this study, the parameters of the fragility curves are obtained using the least-square error method proposed by Baker (*39)*. In this method, the parameters of the lognormal distribution are estimated by minimizing the sum of the squared errors between the observed fractional number of ground motions (z_j/n_j) causing the structure to reach a given damage state and the probability of reaching that damage state as predicted by the fragility function. The method is mathematically described by **Equation 21**.

$$\{\bar{\theta}, \bar{\beta}\} = argmin \sum_{j=1}^{m} \left\{ \frac{z_j}{n_j} - \Phi\left(\frac{\ln(IM_i) - \bar{\theta}}{\bar{\beta}} \right) \right\}^2 \quad (21)$$

3.3 DEMONSTRATION OF FRAMEWORK

An example bridge column designed according to the Caltrans Bridge Design Specifications in 1990 is considered in this study (*40*). The circular column has a diameter of 1829 mm and a height of 6.8 m. The longitudinal reinforcement consists of 58 No. 36 rebars (diameter = 36 mm), and the transverse reinforcement consists of No. 13 stirrups with 76 mm spacing. Geometric and cross-sectional details of the column are shown in **Figure 2**. Fragility analyses were performed for two columns that were identical except for their cover concrete material. The two columns had normal concrete and ECC cover to understand the impact of concrete cover material on seismic fragility of columns exposed to deterioration.

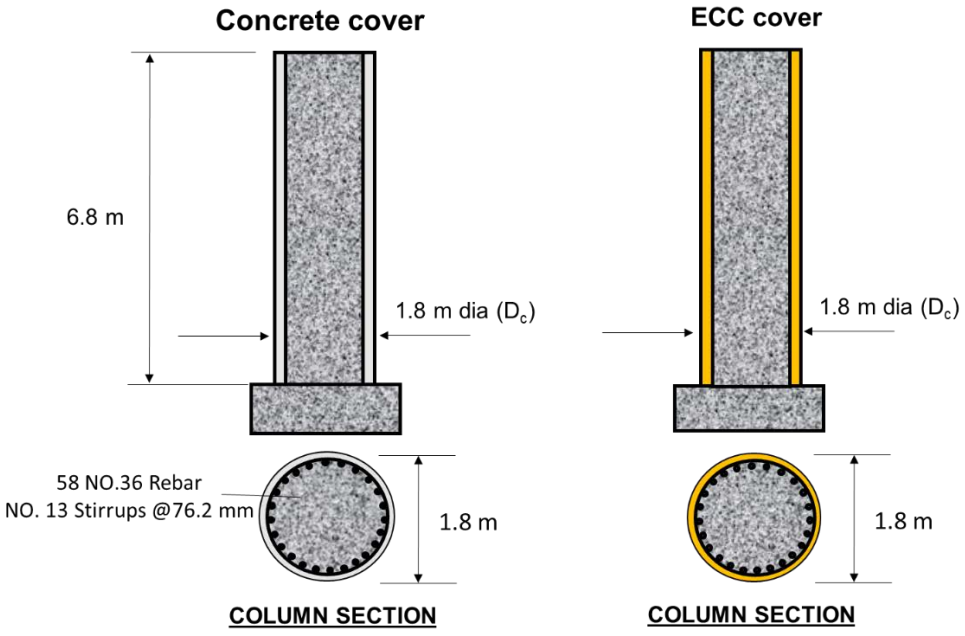

Figure 2 Bridge column detail

3.3.1 Finite element model

A finite element model of the column is created in OpenSEES (*41*). A fiber section model is used to simulate the cross-section of the column. Unconfined concrete properties are assigned to the cover concrete, whereas confined concrete properties are assigned to the core concrete fibers. In this study, differences in corrosion resistance of ECC and normal concrete are considered. However, mechanical properties of ECC cover are assumed the same as those of unconfined concrete cover for simplicity, as the effect of cover concrete on dynamic response is anticipated to be minimal. Reinforced concrete behavior is modeled using the Concrete 07 material model (*42*) in OpenSEES. Reinforcing steel is modeled using the Steel 02 material model in OpenSEES (*43, 44*), including isotropic strain hardening. The unconfined compressive strength of concrete is 35 MPa and the yield strength of reinforcing steel is 414 MPa. **Table 2** shows all the material model parameters and

Figure 3 shows the mesh detail of the column section.

Table 2 Material properties used in the finite element model

Material property	Concrete 07 (Unconfined)	Concrete 07 (Confined)	Steel 02 (Reinforcement)
Compressive strength (MPa)	34.5	39.2	Yield strength = 414 MPa
Strain at compressive strength	0.002	0.0035	
Ultimate comp. strain capacity	0.003	0.011	
Tensile strength (MPa)	3.6	3.6	
Strain at tensile strength	0.0002	0.0002	

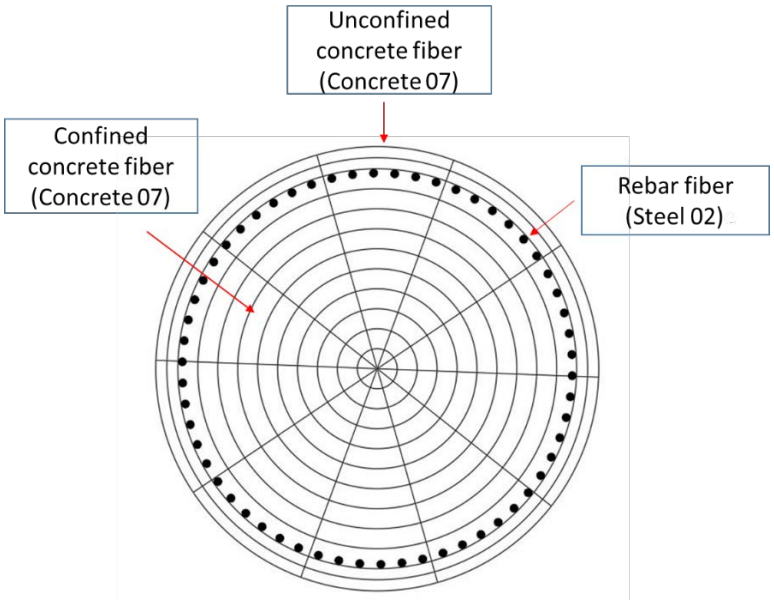

Figure 3 Finite element mesh of the example bridge column

3.3.2 Ground motions

Different ground motions cause different structural responses. For demonstrating the computational framework, 50 ground motion records from the 1994 Northridge earthquake are used. Any other set of ground motions can also be used in this framework. PGA is used to describe the severity of the earthquake ground motion. A large PGA does not necessarily cause severe structural damage; however, using the simple structural model assumed in this study, higher PGA corresponds to higher structural damage. Thus, Northridge ground motions with PGA higher than 100 cm/s^2 were selected and scaled linearly from PGA of 0.1g to 2.0g with increments of 0.1g.

4. FINDINGS

The framework was applied on the example column to demonstrate the effect of deterioration on seismic fragility and the effect of concrete cover material on corrosion susceptibility and seismic fragility.

4.1 Corrosion model results

(a) shows the determination of corrosion initiation time of rebars with concrete and ECC covers. As seen in the figure, corrosion initiates earlier in the transverse rebar than the longitudinal rebar regardless of the cover concrete type. This is attributed to the smaller concrete cover to the transverse rebar than to the longitudinal rebar. The corrosion initiation time for the rebar in ECC cover is longer than that in concrete cover. The ECC cover delays the corrosion initiation time of longitudinal and transverse rebars by 2 years and 3 years, respectively.

(b) shows the rebar area loss due to corrosion as a function of time. Corrosion affects transverse rebar more significantly than the longitudinal rebar regardless of the cover material. For instance, after 100 years, 64% of the original longitudinal rebar area is left, whereas the transverse rebar area completely diminishes due to corrosion with conventional concrete cover. The rebar area loss rate appears to accelerate with time, regardless of the cover material. For instance, in the first 50 years, the average longitudinal rebar area loss rate is 1.7 mm^2/year with concrete cover, which increases to about 5.6 mm^2/year from 50 to 100 years. A similar trend can be observed in the transverse rebar loss rate. ECC cover reduces the rebar area loss rate in both longitudinal and transverse rebars, although the reduction is more significant for the transverse rebar. After 100 years, the longitudinal rebar area left with ECC cover is about 22% larger than that left with normal concrete cover, and the transverse rebar area left with ECC cover is about 37% larger than that left with conventional concrete cover. Thus, the ECC cover significantly enhances the durability of the column as compared to the conventional concrete cover.

Crack width variations with time in longitudinal and transverse directions are shown in **Figure 5**. Although the transverse crack starts earlier than the longitudinal crack with either of the two cover types, the width of the transverse crack increases faster than the longitudinal crack with ECC cover and slower than the longitudinal crack with concrete cover, respectively. Crack widths increase at a much faster rate in conventional concrete cover compared to the ECC cover, which is expected due to the crack bridging effect of the fibers in ECC. Longitudinal cover crack never reaches 1 mm even after 100 years with the ECC cover.

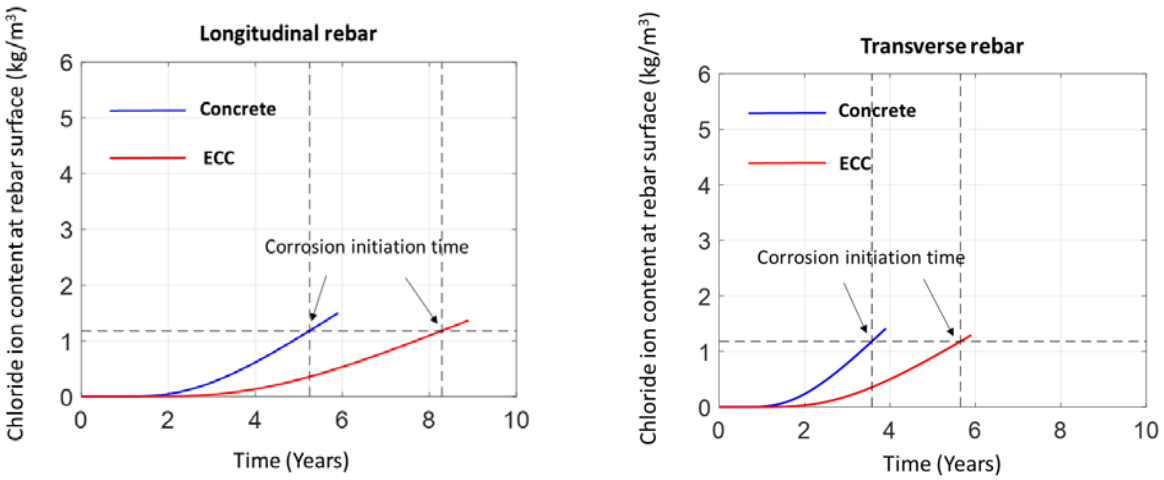

(a) Corrosion initiation

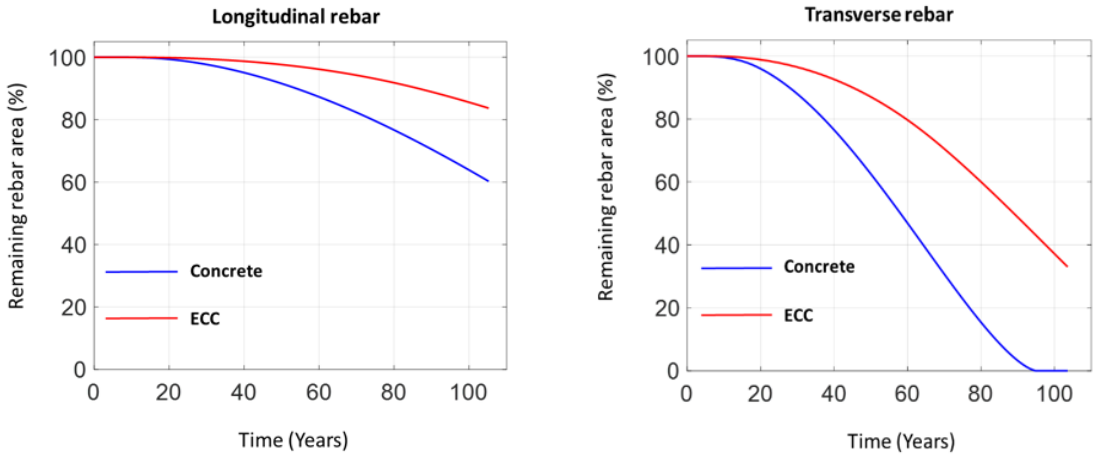

(b) Rebar area loss

Figure 4 Corrosion effects on reinforcement

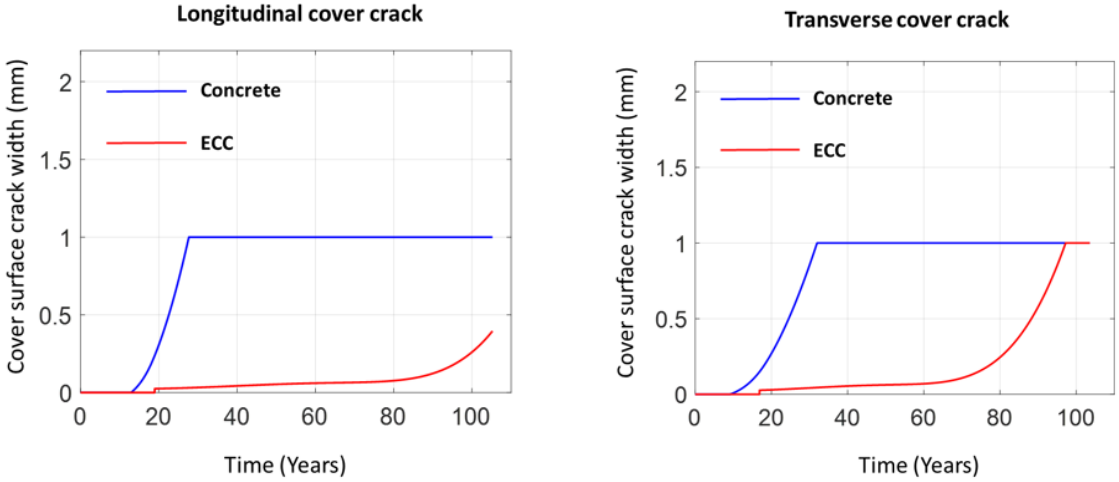

(a) (b)

Figure 5 Longitudinal and transverse cover crack width variation with time

4.2 Time-dependent fragility curves of the example column

Fragility curves of the column with conventional concrete cover are shown in **Figure 6** for a column that is 0 years (newly constructed), 25 years, 50 years and 75 years (end of service life) old. It can be observed that the probability of damage (for a particular damage state) at a given PGA increases with time, as the corrosion effects (rebar mass loss) become more significant with time (

). For instance, at 25 years, the probability of damage is similar to the original state; however, at 50 and 75 years, the probability of damage at a given PGA increases due to corrosion. Furthermore, the corrosion effects become more significant for higher damage states. For instance, the probability of *collapse* of the column for PGA equal to 1.0g at 50 years is about 20% higher than the probability of collapse of a

newly constructed column (at 0 years). In comparison, the probability of *extensive damage* for a 50 year old column is about 6% higher relative to a newly constructed column at PGA of 1.0g.

Figure 7 shows the fragility curves of the same column with ECC cover. Similar to the above observations with conventional concrete cover, the corrosion effects become more significant with time. Corrosion affects higher damage levels more significantly than lower damage levels. In spite of this, the corrosion effects on the fragility curves are reduced with ECC cover compared to conventional concrete cover. At slight and moderate damage levels, there is almost no change in the fragility curves with time in **Figure 7** due to enhanced durability against corrosion offered by the ECC cover.

Figure 8 shows the differences between the fragility curves of the example bridge column obtained with ECC cover and conventional concrete cover at 75 years. Compared to conventional concrete cover, the ECC cover reduces the probability of damage (at all damage levels) due to enhanced durability against corrosion. For instance, at collapse level, the damage probability at PGA equal to 1.0 g with the ECC cover is reduced by about 20% relative to that with conventional concrete cover.

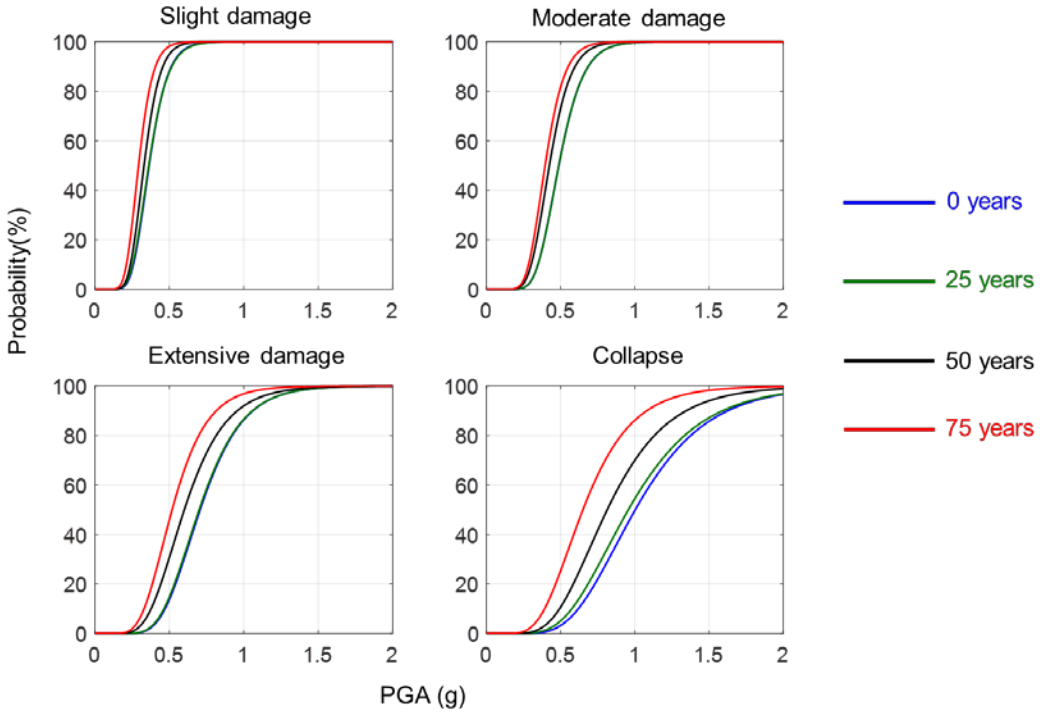

Figure 6 Fragility curves of RC bridge column with conventional concrete cover

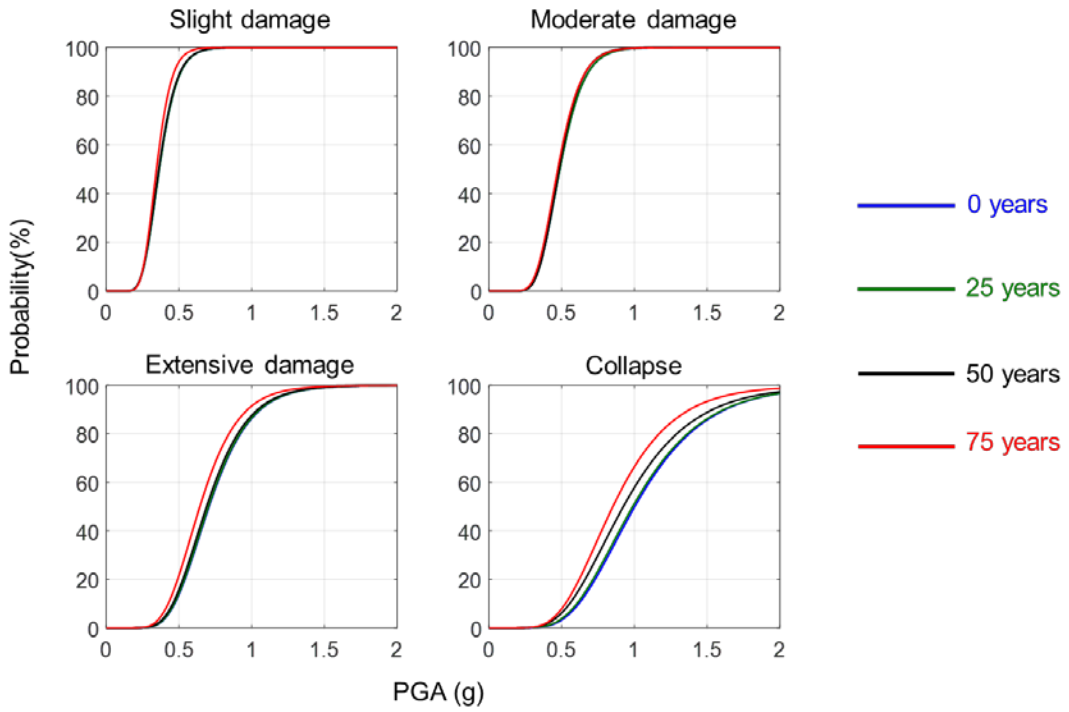

Figure 7 Fragility curves of RC bridge column with ECC cover

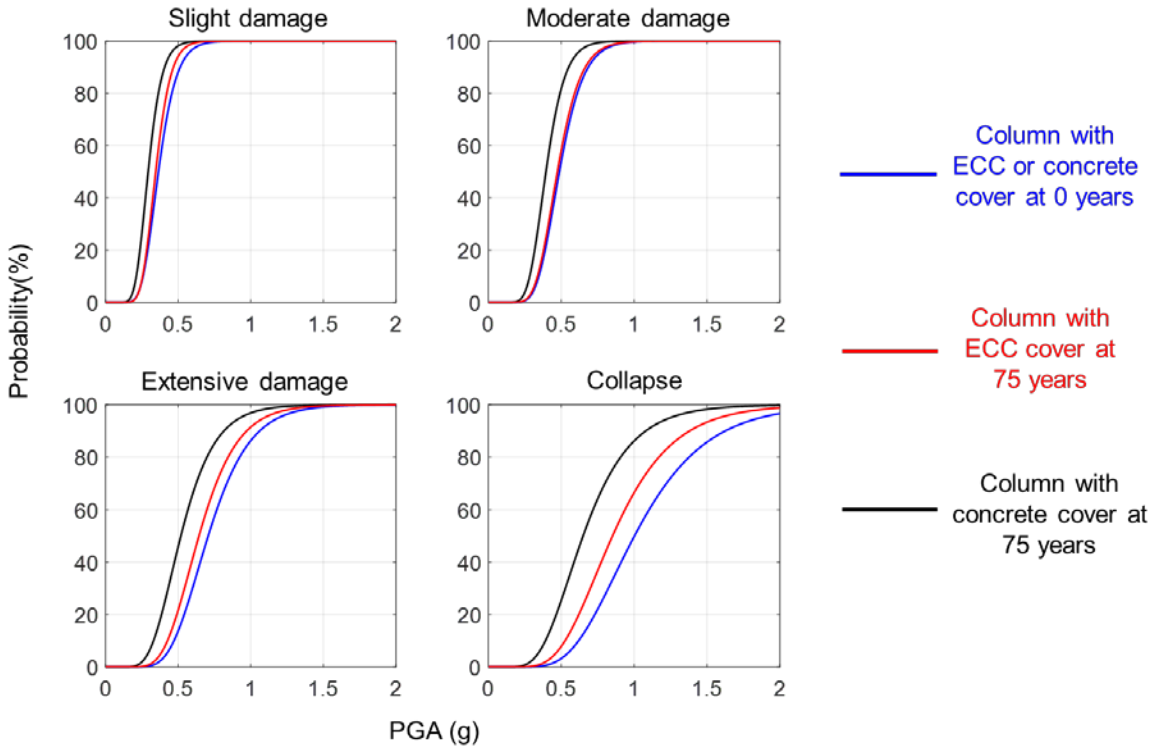

Figure 8 Comparison of fragility curves obtained using conventional concrete and ECC covers at 75 years

5. CONCLUSIONS

This research developed a systematic framework to determine the effect of corrosion deterioration on seismic resilience. The framework utilizes seismic fragility analysis to determine the probability of damage of deteriorating bridge columns under seismic excitation. The framework is demonstrated using an example RC bridge column, analyzed at discrete intervals during its service life. Impact of replacing the conventional concrete reinforcement cover with ductile fiber-reinforced concrete (ECC) reinforcement cover on the fragility is investigated to inform decisions about the use of advanced materials in bridge construction, maintenance and repair. The framework can also be used on a group of bridges to identify most vulnerable bridges to prioritize maintenance.

A novel method to incorporate the influence of multiple cracking in ECC on the corrosion rate is presented. The corrosion model takes into account the effects of pitting corrosion on both longitudinal and transverse rebar and cracking in conventional concrete. This framework can be extended to other deterioration processes and hazards (extreme events) such as vehicle impact or wind with appropriate modifications for hazard modeling.

The following specific conclusions can be drawn based on the results of this study:

1. Lower effective chloride diffusion coefficient of ECC compared to conventional concrete helps delay corrosion initiation (assuming the same critical chloride content).
2. The percent mass loss (relative to the original mass) of the transverse reinforcement is greater than that of the longitudinal reinforcement. This is because the transverse rebar is closer to the external surface of the column than the longitudinal rebar and the original mass of the transverse reinforcement is smaller than that of the longitudinal reinforcement.
3. After crack formation and during corrosion propagation, the corrosion rate is lower with ECC cover than with concrete cover due to better crack width control in ECC.
4. The effects of corrosion become more significant on the seismic performance of the example column with time. The effects of corrosion on seismic fragility are significantly less for the column with ECC cover than with conventional concrete cover.
5. The benefit of corrosion reduction of ECC cover is more pronounced at higher damage levels than lower damage levels.

6. RECOMMENDATIONS

The following recommendations are provided based on the findings of this study:

- Bridge owners should consider time-dependent deterioration (due to corrosion or other mechanisms) for assessing the vulnerability of bridges under extreme hazards, particularly against collapse and extensive damage.
- The asset management teams of state DOTs should consider durability and resilience of structures simultaneously for prioritizing repair and rehabilitation, possibly using their asset management software
- Use of advanced materials that offer better corrosion protection is recommended to not only improve durability but also to increase resiliency. These materials can be used strategically in small amounts (e.g., in reinforced concrete column cover) to limit their higher initial cost.
- Durability and resilience assessments can be improved when transport properties and cracking of advanced materials are characterized and included in the assessment framework.

7. REFERENCES

1. Koch, G. H., M. P. Brongers, N. G. Thompson, Y. P. Virmani, and J. H. Payer. *Corrosion Cost and Preventive Strategies in the United States.* Publication FHWA-RD-01-156, FHWA, U.S. Department of Transportation, 2002.

2. ASCE. *2017 Infrastructure Report Card.* ASCE. https://www.infrastructurereportcard.org. Accessed May 20, 2019.

3. Li, V. C. High-Performance and Multifunctional Cement-Based Composite Material. *Engineering,* Vol. 5, No. 2, 2019, pp. 250-260.

4. Choe, D.-E., P. Gardoni, D. Rosowsky, and T. Haukaas. Seismic Fragility Estimates for Reinforced Concrete Bridges Subject to Corrosion. *Structural Safety,* Vol. 31, No. 4, 2009, pp. 275-283.

5. Akiyama, M., D. M. Frangopol, and H. Matsuzaki. Life-Cycle Reliability of Rc Bridge Piers under Seismic and Airborne Chloride Hazards. *Earthquake Engineering & Structural Dynamics,* Vol. 40, No. 15, 2011, pp. 1671-1687.

6. Ghosh, J., and J. E. Padgett. Aging Considerations in the Development of Time-Dependent Seismic Fragility Curves. *Journal of Structural Engineering,* Vol. 136, No. 12, 2010, pp. 1497-1511.

7. Alipour, A., B. Shafei, and M. Shinozuka. Performance Evaluation of Deteriorating Highway Bridges Located in High Seismic Areas. *Journal of Bridge Engineering,* Vol. 16, No. 5, 2010, pp. 597-611.

8. Stewart, M. G. Mechanical Behaviour of Pitting Corrosion of Flexural and Shear Reinforcement and Its Effect on Structural Reliability of Corroding Rc Beams. *Structural Safety,* Vol. 31, No. 1, 2009, pp. 19-30.

9. Stewart, M. G., and A. Al-Harthy. Pitting Corrosion and Structural Reliability of Corroding Rc Structures: Experimental Data and Probabilistic Analysis. *Reliability engineering & system safety,* Vol. 93, No. 3, 2008, pp. 373-382.

10. Darmawan, M. Pitting Corrosion Model for Reinforced Concrete Structures in a Chloride Environment. *Magazine of Concrete Research,* Vol. 62, No. 2, 2010, p. 91.

11. Ghosh, J., and P. Sood. Consideration of Time-Evolving Capacity Distributions and Improved Degradation Models for Seismic Fragility Assessment of Aging Highway Bridges. *Reliability engineering & system safety,* Vol. 154, 2016, pp. 197-218.

12. Afsar Dizaj, E., R. Madandoust, and M. M. Kashani. Exploring the Impact of Chloride-Induced Corrosion on Seismic Damage Limit States and Residual Capacity of Reinforced Concrete Structures. *Structure and Infrastructure Engineering,* Vol. 14, No. 6, 2018, pp. 714-729.

13. Cui, F., H. Zhang, M. Ghosn, and Y. Xu. Seismic Fragility Analysis of Deteriorating Rc Bridge Substructures Subject to Marine Chloride-Induced Corrosion. *Engineering Structures,* Vol. 155, 2018, pp. 61-72.

14. Biondini, F., E. Camnasio, and A. Palermo. Lifetime Seismic Performance of Concrete Bridges Exposed to Corrosion. *Structure and Infrastructure Engineering,* Vol. 10, No. 7, 2014, pp. 880-900.

15. Otieno, M., M. Alexander, and H.-D. Beushausen. Corrosion in Cracked and Uncracked Concrete–Influence of Crack Width, Concrete Quality and Crack Reopening. *Magazine of Concrete Research,* Vol. 62, No. 6, 2010, pp. 393-404.

16. Cao, C., M. M. Cheung, and B. Y. Chan. Modelling of Interaction between Corrosion-Induced Concrete Cover Crack and Steel Corrosion Rate. *Corrosion Science,* Vol. 69, 2013, pp. 97-109.

17. Li, V. C. On Engineered Cementitious Composites: A Review of the Material and Its Applications. *Journal of Advanced Concrete Technology,* Vol. 1, No. 3, 2003, pp. 215-230.

18. Miyazato, S., and Y. Hiraishi. Transport Properties and Steel Corrosion in Ductile Fiber Reinforced Cement Composites.In *Proceedings of the Eleventh International Conference on Fracture*, 2005. pp. 20-25.

19. Sahmaran, M., M. Li, and V. C. Li. Transport Properties of Engineered Cementitious Composites under Chloride Exposure. *ACI Materials Journal,* Vol. 104, No. 6, 2007, pp. 604-611.

20. Lepech, M. D., and V. C. Li. Water Permeability of Engineered Cementitious Composites. *Cement and Concrete Composites,* Vol. 31, No. 10, 2009, pp. 744-753.

21. Mihashi, H., S. F. U. Ahmed, and A. Kobayakawa. Corrosion of Reinforcing Steel in Fiber Reinforced Cementitious Composites. *Journal of Advanced Concrete Technology,* Vol. 9, No. 2, 2011, pp. 159-167.

22. Fakhri, H. *Corrosion Mitigation in Reinforced Concrete Structures Using Engineered Cementitious Composites*, PhD dissertation, Department of Civil, Structural and Environmental Engineering, University at Buffalo, The State University of New York, 2019.

23. Wang, S., and V. C. Li. Engineered Cementitious Composites with High-Volume Fly Ash. *ACI Materials Journal,* Vol. 104, No. 3, 2007, pp. 233-241.

24. Crank, J. *The Mathematics of Diffusion*. Oxford University Press, Oxford, UK, 1979.

25. Bertolini, L., B. Elsener, P. Pedeferri, E. Redaelli, and R. Polder. *Corrosion of Steel in Concrete: Prevention, Diagnosis, Repair*. WILEY-VCH Verlag GmbH & Co. KGaA, Weinheim, 2004.

26. Val, D. V., and R. E. Melchers. Reliability of Deteriorating Rc Slab Bridges. *Journal of Structural Engineering,* Vol. 123, No. 12, 1997, pp. 1638-1644.

27. Du, Y., L. Clark, and A. Chan. Residual Capacity of Corroded Reinforcing Bars. *Magazine of Concrete Research,* Vol. 57, No. 3, 2005, pp. 135-147.

28. El Maaddawy, T., and K. Soudki. A Model for Prediction of Time from Corrosion Initiation to Corrosion Cracking. *Cement and Concrete Composites,* Vol. 29, No. 3, 2007, pp. 168-175.

29. Vidal, T., A. Castel, and R. Francois. Analyzing Crack Width to Predict Corrosion in Reinforced Concrete. *Cement and Concrete Research,* Vol. 34, No. 1, 2004, pp. 165-174.

30. Molina, F., C. Alonso, and C. Andrade. Cover Cracking as a Function of Rebar Corrosion: Part 2—Numerical Model. *Materials and structures,* Vol. 26, No. 9, 1993, pp. 532-548.

31. Liu, T., and R. Weyers. Modeling the Dynamic Corrosion Process in Chloride Contaminated Concrete Structures. *Cement and Concrete Research,* Vol. 28, No. 3, 1998, pp. 365-379.

32. Ranade, R., J. Zhang, J. P. Lynch, and V. C. Li. Influence of Micro-Cracking on the Composite Resistivity of Engineered Cementitious Composites. *Cement and concrete research,* Vol. 58, 2014, pp. 1-12.

33. Li, W., W. Liu, and S. Wang. The Effect of Crack Width on Chloride-Induced Corrosion of Steel in Concrete. *Advances in Materials Science and Engineering,* Vol. 2017, 2017.

34. Life-365™. *Life-365 Service Life Predication Model*^{tm}. Life-365 Consortium. http://www.life-365.org. Accessed Sep. 9, 2018.

35. Broomfield, J. P. *Corrosion of Steel in Concrete: Understanding, Investigation and Repair*. Taylor & Francis, New York, 2007.

36. Cheng, H., H.-N. Li, Y. Yang, and D.-S. Wang. Seismic Fragility Analysis of Deteriorating Rc Bridge Columns with Time-Variant Capacity Index. *Bulletin of Earthquake Engineering,* 2019, pp. 1-21.

37. Vamvatsikos, D., and C. A. Cornell. Incremental Dynamic Analysis. *Earthquake Engineering & Structural Dynamics,* Vol. 31, No. 3, 2002, pp. 491-514.

38. Paulay, T., and M. N. Priestley. *Seismic Design of Reinforced Concrete and Masonry Buildings*. John Wiley & Sons, Inc., New York, 1992.

39. Baker, J. W. Efficient Analytical Fragility Function Fitting Using Dynamic Structural Analysis. *Earthquake Spectra,* Vol. 31, No. 1, 2015, pp. 579-599.

40. Ramanathan, K. N. *Next Generation Seismic Fragility Curves for California Bridges Incorporating the Evolution in Seismic Design Philosophy*, PhD Dissertation, Georgia Institute of Technology, 2012.

41. McKenna, F., G. L. Fenves, and M. H. Scott. *Open System for Earthquake Engineering Simulation.* University of California, Berkeley, California. http://opensees.berkeley.edu. Accessed Sep. 1, 2018.

42. Chang, G., and J. B. Mander. Seismic Energy Based Fatigue Damage Analysis of Bridge Columns: Part 1-Evaluation of Seismic Capacity.In, National Center For Earthquake Engineering Research, 1994.

43. Menegotto, M. Method of Analysis for Cyclically Loaded Rc Plane Frames Including Changes in Geometry and Non-Elastic Behavior of Elements under Combined Normal Force and Bending.In *Proc., IABSE symposium on resistance and ultimate deformability of structures acted on by well defined repeated loads*, 1973. pp. 15-22.

44. Filippou, F. C., V. V. Bertero, and E. P. Popov. Effects of Bond Deterioration on Hysteretic Behavior of Reinforced Concrete Joints.In, Earthquake Engineering Research Center, 1983.